BIFURCATION OF FLOW AROUND A ROTATING DISK

T. WATANABE[1c], H. FURUKAWA[2]

[1]Graduate School of Information Science, Nagoya University, Nagoya, 464-8601, Japan
[2]Facculty of Engineering, Meijo University, Nagoya, 468-8502, Japan

[c]Corresponding author: Tel.: +81527894785; Fax: +81527894785; Email: takashi@is.nagoya-u.ac.jp

KEYWORDS:
Main subjects: rotating flow, outer casing, flow visualization
Fluid: flow transition, flow state change
Visualization method(s): computer-based visualization
Other keywords: image processing, flows at low to high Reynolds numbers

ABSTRACT: We investigate the flow around a rotating disk in a cylindrical casing. The thickness of the disk is finite and its radius is smaller than the inner radius of the casing. Therefore, the flow field has an axial gap and the radial gap. This is more realistic model of fluid machinery than the flow field that has only an axial gap or a rotating container. Because the disk has a finite thickness, Taylor-Couette like flow appears at the radial gap. The study is carried out by the direct numerical simulation based on the Navier-Stokes equations and the equation of continuity. The Reynolds number Re is based on the disk radius and the rotating speed of the disk rim. When the Reynolds number is small, steady Taylor vortices appear at the radial gap. At Re = 7000, six or seven vortices appear around the disk rim. These vortices make a time variation of torque acting on the disk. Therefore, this flow type is not preferable for the safety operation of fluid machinery. When the Reynolds number is 8000, small vortices appear around the disk rim. The number of the vortices is about 30. In this case, flow is stable and no variation of the torque appears. When the flow develops further and the Reynolds number is 12000 or above, the vortices propagate into the inner region of the disk and they make a spiral rolls with negative front angle. We show that five flow patterns emerge. From a detail calculation, the critical Reynolds numbers among the appearances of these flow patterns are determined.

Introduction

Rotating flows found in hard disk drives and various kinds of fluid machinery are important flows in fluid dynamics, and experimental and numerical studies have been carried out[1, 2]. In these flows, flow patterns of basic flows, circular flows, spiral rolls, turbulent spirals and turbulent flows appear as the Reynolds number increases[3].

The studies on these flows are classified in three categories. The first is the flow around a rotating disk in a cylindrical casing. The radius of the disk and the inner radius of the casing are almost same. The axial gap between the disk surface and the end wall of the casing is narrow. This gives a cross flow model. In this case, Cross et al.[4] experimentally showed the circular rolls, spiral rolls and the spots in the turbulent flow. The second is the flows in the rotating container and the rotating annular cavity. Lopez et al.[5] shows the instabilities in the Bödewat layer on a stationary end wall. Hung et al.[6] used the PIV method and measured the core flow around the hub connecting two rotating disks. The third is the flows around a rotating disk with the radial gap as well as the axial gap in a cylindrical casing. Schouveiler et al.[7] experimentally showed the effect of the radial gap is large on the flow near the disk rim. While these flows give more realistic models of fluid machinery, the studies of these flows are limited and the effects of the radial gap and the Reynolds number are not clear. Here, we numerically investigate this third flow.

When the disk has a finite thickness, Taylor-Couette-like flow appears between the disk rim and the side wall of the casing and this originates a new instability of the flow. We have investigated the effect of this instability by the numerical and experimental approaches[8, 9]. As the Reynolds number increases, steady Taylor-Couette flow, sickle-like vortices, bead-like vortices, spiral rolls appear at the radial gap and around the disk rim. However the results of our studies are a little bit qualitative. In this paper, we carried out more detail calculation and defined the criterions that determine which flow pattern appears in the flow field.

Formulation

The schematic flow field and the cylindrical coordinate system (r, θ, z) are shown in Fig. 1. The disk is placed at the middle of the cylindrical casing and it is rotated by a driving shaft. The z axis is aligned with the driving shaft and the origin of the coordinate system is placed at the center of the bottom end wall of the casing. The radius and the length of the casing are denoted by r_c and h_c, respectively. The radius and the thickness of the rotating disk are represented by r_d and h_d, respectively. The upper and lower axial gaps (h_u and h_l) are identical. The reference length is the radius of the disk and the reference velocity is the azimuthal velocity at the rim of the disk (v_d). These reference values are used to evaluate the Reynolds number and to make dimensionless quantities. In out experiment, following geometrical values are used:

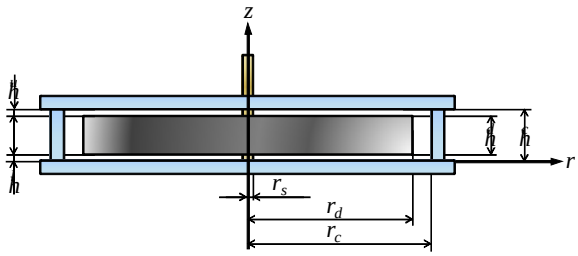

Fig.1 Flow field and coordinate system.

$r_c = 1.1181$, $h_c = 0.3150$, $r_d = 1.0$, $h_d = 0.2362$, $h_u = h_l = 0.0394$.

In our experiment[8], these values stand for the inner radius of the casing of 142 mm, the length of the casing of 40 mm, the disk radius of 127 mm and the disk thickness of 30 mm.

The governing equations are the equation of continuity and the three-dimensional Navier-Stokes equations,

$$\nabla \cdot \mathbf{u} = 0$$

$$\frac{\partial \mathbf{u}}{\partial t} + \nabla(\mathbf{u}\mathbf{u}^T) = -\nabla p + \frac{1}{\mathrm{Re}} + \Delta \mathbf{u}$$

where the velocity vector $\boldsymbol{u} = (u, v, w)^T$, t is time, p is pressure and Re is the Reynolds number given by $v_d\, r_d/\nu$ (ν is the kinematic viscosity).

The boundary condition is the no-slip condition on the wall. The flow is at rest in the initial condition and the disk suddenly begins to rotate to give a prescribed Reynolds number.

The continuous equations are discretized by the finite difference method. The convection terms are modeled by the QUICK method. The MAC method is used and the staggered grid is introduced. This is helpful to remove singularities at the connecting point between the rotating driving shaft and the stationary end wall of the casing. The representative grid points are 265 in the radial direction, 338 in the azimuthal direction and 81 in the axial direction. It was confirmed that these grid points are enough to evaluate the flow shown in this paper.

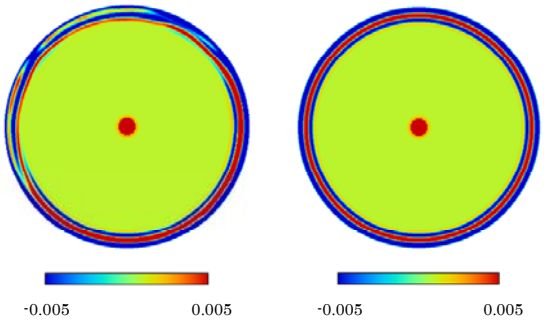

$t = 60$ $t = 200$

Fig. 2 Contour of the axial velocity component in the r-θ plane (Re = 6300, z = 0.00984).

Steady flow at Reynolds number 6300

The flow at relatively small Reynolds number of 6300 is shown in Fig. 2 and Fig. 3. Figure 2 shows the contour of the axial velocity component shown from z direction. The disk is rotating in the counter-clockwise direction. At t = 60, the flow is in the developing state. The well developed flow is established at t = 200, that is almost axisymmetric.

Figure 3 represents the contour of the axial velocity

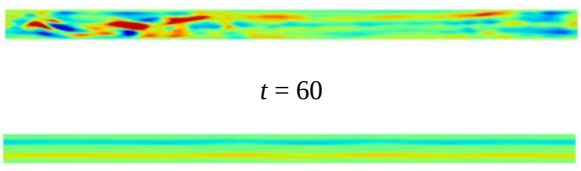

$t = 60$

$t = 200$

Fig. 3 Contour of the axial velocity component in the θ-z plane in the radial gap (Re = 6300, r = 1.06).

component at a fixed radial position of r = 1.06 where is in the axial gap. The horizontal direction is the azimutal angle from 0 to 2π, and the vertical direction is the axial direction. The well developed flow at t = 200 has variations parallel to the azimuthal direction.

The flows in the r-z plane near the radial gap are shown in Fig. 4. The horizontal direction is the radial direction and the vertical direction is the axial direction. Black lines in the figure represent the rotating disk. In the developing flow at t = 60, three main vortices attached with a small vortex at the upper end appear. In the well-developed flow at t = 200, steady four vortices appear in the radial gap. Boundary layers develop on the rotating disk and the end wall of the casing. Velocity vectors of them are also shown in Fig. 4. These boundary layers are merged and no core region is found.

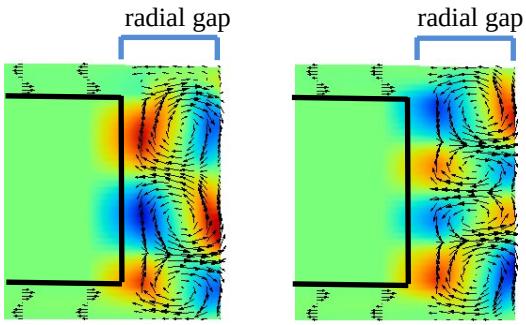

t = 60 t = 200

Fig. 4 Contour of the axial velocity component in the r-z plane (Re = 6300, θ = 0.0).

Sickle-like flow at Reynolds number 7000

The flow at Re = 7000 is shown in Figs. 5, 6 and 7. Figure 5 represents the contour of the axial velocity component in the r-θ plane. Small vortices appear around the disk rim at t = 70. The number of vortices is about thirty. We call this vortex a bead-like vortex and the flow with bead-like vortices a bead-like flow. At Re = 7000, the bead-like flow is not permanent. The small vortices begin to merge with each other and a large vortex named by a sickle vortex appears. The flow with large vortices at t = 230 is shown in the right panel of Fig. 5.

The flows at r = 1.06 are given in Fig. 6. At t = 70, bead-like flow appears and the small vortices are confined to the one side of the end wall of the cylindrical casing. Similarly, while the sickle-like flow with several sickle vortices at t = 230 has a larger flow structure than that of the bead-like flow, it is not symmetric with respect to the axial direction neither. The vortices only on the one side of the casing made an oscillation of the entire flow and the

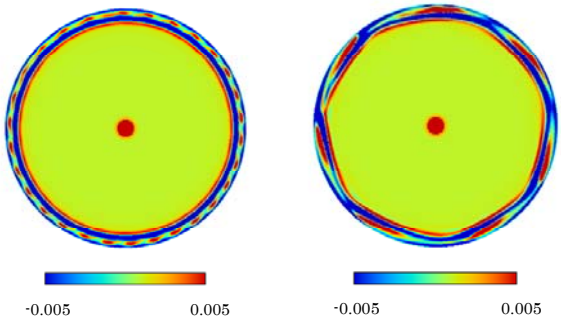

t = 70 t = 230

Fig. 5 Contour of the axial velocity component in the r-θ plane (Re = 7000, z = 0.00984).

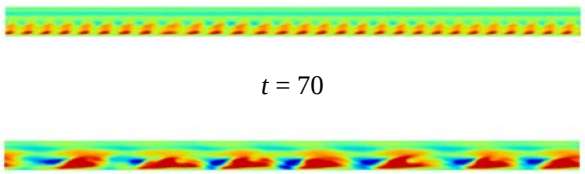

t = 70

t = 230

Fig. 6 Contour of the axial velocity component in the θ-z plane in the radial gap (Re = 7000, r = 1.06).

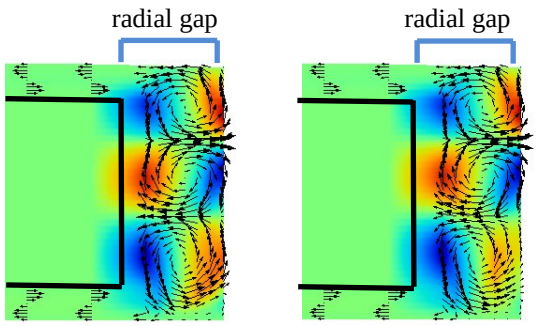

θ = 0.374 [rad] θ = 0.524 [rad]

Fig. 7 Contour of the axial velocity component in the r-z plane at two azimuthal positions (Re = 7000, t = 70).

torque acting on the disk and the energy in the flow region changed with time.

Figure 7 shows the flows in the *r*-*z* plane at different azimuthal position. The time *t* is 70. Differing from the well developed flow at Re = 6300, three vortices appear in the radial gap, and this also suggest the asymmetry of the flow. The flow pattern changes at each azimuthal section. In the experiment, the change of flow pattern appears as the time variation of the flow structure.

Bead-like flow at Reynolds number 8000

When the Reynolds number is 8000, well developed flow has a structured pattern. They are shown in Figs. 8, 9 and 10. In this case, well formed bead-like flow appears at the early time of the numerical simulation. Figure 8 shows the flows near the two end walls of the cylindrical casing. Though the sign of the values of the axial velocity component is different at two different *z* (axial) positions, the bead-like flows are found in these figures.

Figure 9 shows the flows at *r* = 1.07 (near the center of the radial gap) and 1.09 (neat the outer edge of the radial gap) in the θ-*z* plane. The bead-like vortices appear on both end walls of the cylindrical casing. The strength of the axial velocity component is stronger at the outer region than that at the middle of the radial gap.

The flows at two azimuthal sections are shown in Fig. 10. The panel at θ = 0.430 [rad] represents the flow including the bead-like vortices, and the panel at θ = 0.430 [rad] gives the flow pattern between the bead-like vortices. Two main vortices appear in the radial gap. At θ = 0.430 [rad], very weak flows appear at corners between the side wall and upper and lower end wall of the casing. When we compare the flows in Fig. 10 with the flows in Fig. 9, we can say that these weak flows correspond to the bead-like vortices.

Following the movement of the bead-like vortices, the flow fluctuates periodically. The reason why the flow does not change to the other mode such as a sickle-like flow is now under consideration.

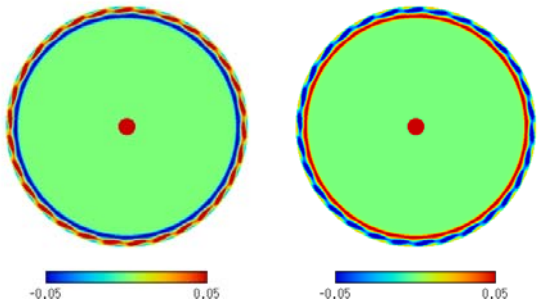

z = 0.0374 *z* = 0.278

Fig. 8 Contour of the axial velocity component in the *r*-θ plane at two axial positions (Re = 8000, *t* = 200).

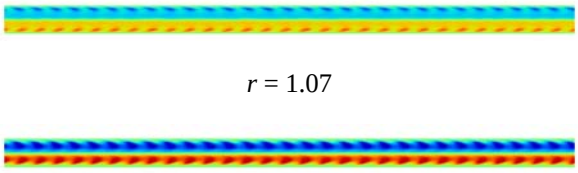

r = 1.07

r = 1.09

Fig. 9 Contour of the axial velocity component in the θ-*z* plane at two positions in the radial gap (Re = 8000, *t* = 200).

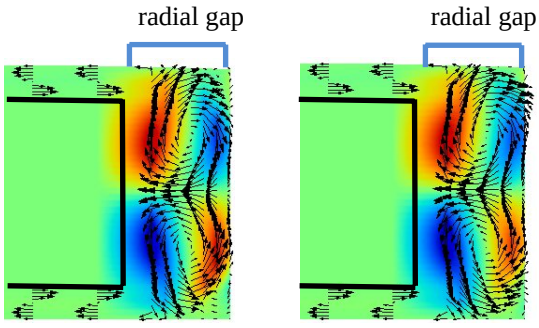

θ = 0.430 [rad] θ = 0.467 [rad]

Fig. 10 Contour of the axial velocity component in the *r*-*z* plane at two azimuthal positions (Re = 7000, *t* = 200).

Bead-like flows with spiral rolls at Reynolds number 12000

When the Reynolds number increases further, spiral rolls with negative front angle appear. In out numerical simulation, spiral rolls appear in the flow at Re = 12000. Figure 11 shows the flows at *z* = 0.00984 and *z* = 0.0374. The rotating direction of the disk is counter-clockwise. The flow at *z* = 0.00984 is that very close to the stationary end wall casing and it is in the Bödewadt layer. The axial position at *z* = 0.0374 is close to the rotating disk and the flow is in the Ekman layer. The spiral rolls are well formed in the Bödewadt layer. The front line of the spiral is opposite to the rotating direction of the disk. Therefore the front angle is negative.

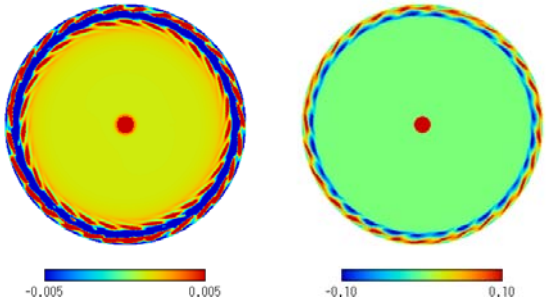

z = 0.00984 z = 0.0374

Fig. 11 Contour of the axial velocity component in the r-θ plane at two axial positions (Re = 12000, t = 300).

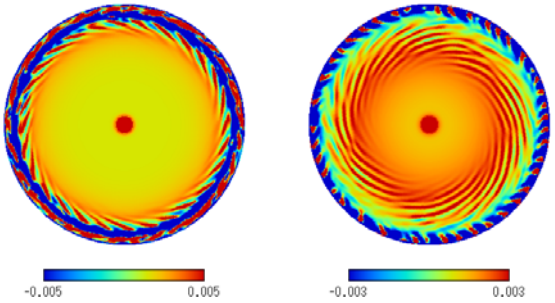

Re = 20000 (radial gap) Re = 55000 (no radial gap)

Fig. 14 Contour of the axial velocity component in the r-θ plane (z = 0.00984, t = 300).

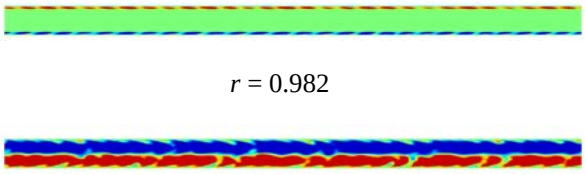

r = 0.982

r = 1.09

Fig. 12 Contour of the axial velocity component in the θ-z plane at two radial positions (Re = 12000, t = 300).

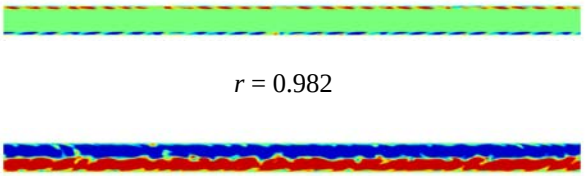

r = 0.982

r = 1.09

Fig. 15 Contour of the axial velocity component in the θ-z plane at two radial positions (Re = 20000, t = 300).

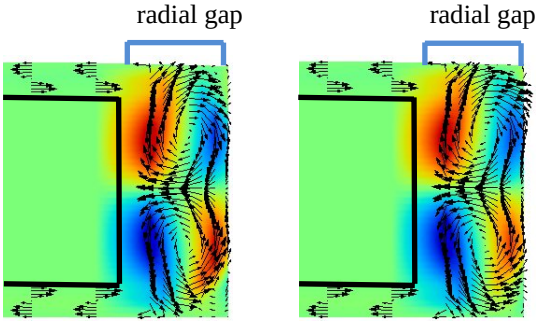

θ = 0.112 [rad] θ = 0.860 [rad]

Fig. 13 Contour of the axial velocity component in the r-z plane at two azimuthal positions (Re = 12000, t = 300).

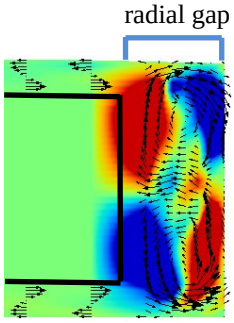

θ = 0.860 [rad]

Fig. 16 Contour of the axial velocity component in the r-z plane (Re = 20000, t = 300).

This result coincides with that given experimentally by ref. (3) and (8). Beside the spiral rolls, bead-like vortices appear both in the Bödewadt layer and the Ekman layer.

The flow structures in the θ-z plane are presented in Fig. 12. Please note that the r = 0.928 corresponds not in the radial gap but on the rotating disk. Periodical pattern of spiral rolls is found on the disk. In the radial gap of r = 1.09, bead-like vortices appear on the both side of the end walls of the casing, though the bead structure is a little bit deformed.

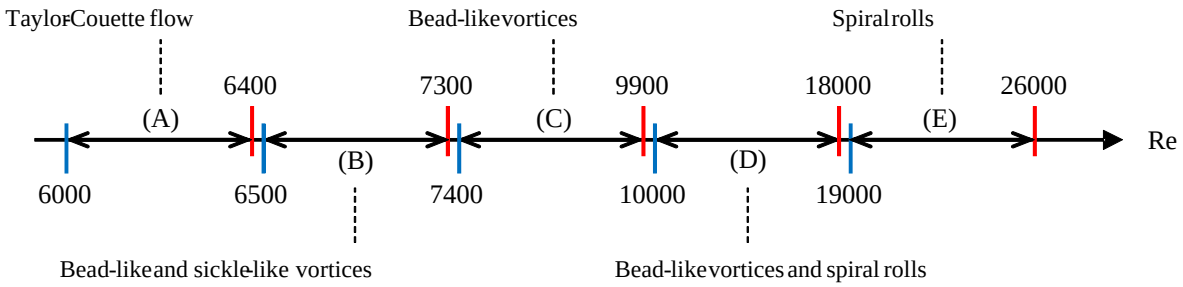

Fig. 17 Bifurcation diagram of the flow with the Reynolds number.

The side flow in Fig. 13 is not much different from that in Fig. 10. However, the fluctuation of the two main vortices is stronger and the disturbances generated by this fluctuation penetrate inward and makes the spiral rolls.

Spiral rolls at Reynolds number 20000

When the Reynolds number is 20000, bead-like flow disappears and spiral rolls extend. The left panel in Fig. 14 gives the flow shown from the axial direction. The spiral rolls have a negative front angle. The right panel in Fig. 14 is the flow when there is no axial gap and the Reynolds number is 55000. The flow with no axial gap shows the spiral rolls with a positive front angle. This flow is also experimentally found [3), (4)].

The flow in θ-z plane is shown in Fig. 15. On the rotating disk at r = 0.982, the periodic sections of the spiral rolls appear, while the flow in the radial gap (r = 1.09) does not have a well-formed flow structure.

The flow in the azimuthal section has a very strong unsteady two vortices flow. These vortices provide much more disturbances and clearer spiral rolls in the inner region.

Bifurcation diagram

In the above sections, we have shown five flow patterns. The first (A) is Taylor-Couette flow in the radial gap. The second (B) forms a bead-like flow and then changes to the sickle-like flow. The third (C) is the bead-like flow independent from the time. The forth (D) is the coexisting flow of the bead-like flow and the spiral rolls with a negative front angle. The fifth (E) is the extended spiral rolls and no well formed bead-like flow appears. Careful calculations confine the critical Reynolds numbers between flow patterns from (A) to (E) within an accuracy of one hundred. As was noted in the section of formulation, the initial state includes the flow at rest in the entire region. Then the disk begins to rotate suddenly to give a prescribed Reynolds number. The bifurcation diagram is shown in Fig. 17. The blue line denotes the lower limit of a flow pattern, and the red line represents the upper limit of a flow pattern. The flow patterns are clear divided by the Reynolds number.

Conclusion

The flow around a rotating disk in a cylindrical casing is numerically predicted. The disk has a finite thickness. The disk radius is smaller than the inner radius of the casing, and the flow configuration has a radial gap as well as an axial gap. In the radial gap, Taylor-Couette like flow appears. When the Reynolds number is small, Taylor-Couette flow is steady. However, as the Reynolds number increases, the flow in the radial gap begins to oscillate with time. Then, the sickle-like vortices and the bead-like vortices appear. At much higher Reynolds number, spiral rolls appear on the stationary end wall of the casing and at the inner region of the disk. These spiral rolls have a negative front angle with respect to the rotating direction of the disk. Five flow patterns are found and the critical Reynolds numbers for the appearance of these flow patterns are determined. One main future study is the verification of these flow patterns and the critical Reynolds number in experiments. In this study, only one geometrical configuration is considered and the only one situation in that the disk is suddenly spun up is evaluated. Therefore, the flow patterns different from the ones

obtained in the current calculation may be obtained when the geometrical size is changed and the way of the increase of decrease of the spinning angular velocity is modified.

References

1. O. Savas, *Stability of Bödewadt flow*, J. Fluid Mech., 1987, **183**, pp. 77-94.
2. E. Serre, P. Bontoux, B. E. Launder, *Direct Numerical Simulation of Transitional Turbulent Flow in a Closed Rotor-Stator Cavity*, Turbulence and Combustion, 2002, **69**, 1, pp. 35-50.
3. L. Schouveiler, P. Le Gal, M. P. Chauve, *Instabilities of the flow between a rotating and stationary disk*, J. Fluid Mech.,2001, **443**, pp. 329-350.
4. A. Cros, E. Floriani, P. Le Gal, R. Lima, *Transition to turbulence of the Batchelor flow in a rotor/stator device*, European J. Mechanics B/Fluid, 2005, **24**, pp. 409-424.
5. J.M. Lopez, F. Marques, A. M. Rubio, M. Avila, *Crossflow instability of finite Bödewadt flows: Transients and spiral waves*, Phys. Fluids, 2009, **21**, 114107.
6. R. F. Huang, M. K. Hsieh, *Phase-resolved flow characteristics between two shrouded co-rotating disks*, Experiments in Fluids, 2011, **51**, 6, pp. 1529-1547.
7. L. Schouveiler, P. Le Gal, M. P. Chauve, *Instabilities of the flow between a rotating and stationary disk*, J. Fluid Mech., 2001, **443**, pp. 329-350.
8. T. Watanabe and H. Furukawa, *Flows around a rotating disks with and without rim-shroud gap*, Experiments in Fluids, 2010, **48**, 4, pp. 631-636.
9. T. Watanabe, and H. Furukawa, *The effect of rim-shroud gap on the spiral rolls formed around a rotating disk*, Phys. Fluids, 2010, **22**, pp. 114107-1-7.